ACS APPLIED MATERIALS & INTERFACES

Research Article

www.acsami.org

Highly Conductive $Cu_{2-x}S$ Nanoparticle Films through Room-Temperature Processing and an Order of Magnitude Enhancement of Conductivity via Electrophoretic Deposition

Obafemi O. Otelaja,[†] Don-Hyung Ha,[‡] Tiffany Ly,[‡] Haitao Zhang,[‡] and Richard D. Robinson*[,‡]

[†]School of Electrical and Computer Engineering, Cornell University, Ithaca, New York 14853, United States

[‡]Department of Materials Science and Engineering, Cornell University, Ithaca, New York 14853, United States

Supporting Information

ABSTRACT: A facile room-temperature method for assembling colloidal copper sulfide ($Cu_{2-x}S$) nanoparticles into highly electrically conducting films is presented. Ammonium sulfide is utilized for connecting the nanoparticles via ligand removal, which transforms the as-deposited insulating films into highly conducting films. Electronic properties of the treated films are characterized with a combination of Hall effect measurements, field-effect transistor measurements, temperature-dependent conductivity measurements, and capacitance–voltage measurements, revealing their highly doped p-type semiconducting nature. The spin-cast nanoparticle films have carrier concentration of $\sim 10^{19}$ cm^{-3}, Hall mobilities of ~3 to 4 $cm^2 V^{-1} s^{-1}$, and electrical conductivities of ~5 to 6 $S \cdot cm^{-1}$. Our films have hole mobilities that are 1–4 orders of magnitude higher than hole mobilities previously reported for heat-treated nanoparticle films of HgTe, InSb, PbS, PbTe, and PbSe. We show that electrophoretic deposition (EPD) as a method for nanoparticle film assembly leads to an order of magnitude enhancement in film conductivity (~75 $S \cdot cm^{-1}$) over conventional spin-casting, creating copper sulfide nanoparticle films with conductivities comparable to bulk films formed through physical deposition methods. The X-ray diffraction patterns of the $Cu_{2-x}S$ films, with and without ligand removal, match the Djurleite phase ($Cu_{1.94}S$) of copper sulfide and show that the nanoparticles maintain finite size after the ammonium sulfide processing. The high conductivities reported are attributed to better interparticle coupling through the ammonium sulfide treatment. This approach presents a scalable room-temperature route for fabricating highly conducting nanoparticle assemblies for large-area electronic and optoelectronic applications.

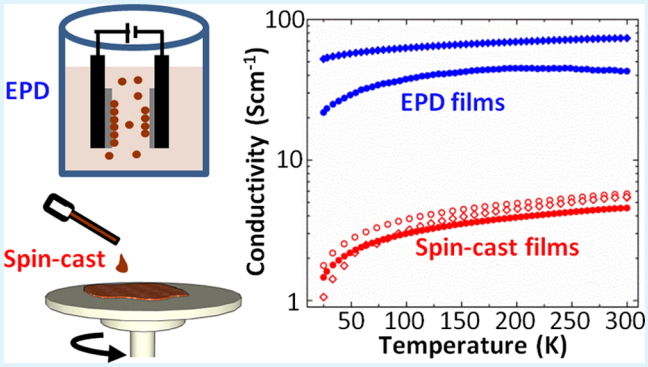

KEYWORDS: *nanoparticle films, electrophoretic deposition, conductivity, hopping transport, copper sulfide*

INTRODUCTION

The need for solution-based processing of semiconductor electronics has spurred interesting research efforts in recent years. In addition to the lower cost for solution processing, it also allows for large-area and flexible electronic applications compared to conventional semiconductor processing methods. Due to their exceptional size-dependent electronic properties and solution processability, semiconducting colloidal nanoparticles are becoming important building blocks for electronic and optoelectronic devices such as field-effect transistors,[1] photovoltaic devices,[2] and light-emitting diodes.[3] These nanoparticles have typically been assembled into thin films with short-range ordering via drop-casting, spin-casting, or inject printing.[4,5] Spin-casting is a widely known method for assembling nanoparticle films from colloidal solution, and the quality of the resulting films depends on appropriate solvent selection and substrate preparation procedures.[4] For practical large-area applications, the spin-casting process results in inefficient use of starting colloidal nanoparticles because a significant portion of the nanoparticle solution is discarded during the process. In addition, obtaining uniform films over a large area is a challenge.

Electrophoretic deposition (EPD) is an alternate method for the fabrication of nanoparticle films that shows great promise for electronic applications.[6,7] EPD has been widely used for the processing of thin films and coatings for a wide variety of novel applications. EPD is accomplished by applying a voltage between two conducting electrodes immersed in a solution containing nanoparticles. The resulting electric field drives the charged particles through the solution, onto electrodes of opposite polarity. EPD is an attractive method for depositing nanoparticle films for applications due to its versatility for fabricating a wide variety of films of different materials, its efficient use of the colloidal particles (most particles in solution

Received: July 21, 2014
Accepted: September 29, 2014
Published: October 14, 2014

are deposited), and the possibility of depositing films on substrates of arbitrary size and geometry. EPD has been shown to result in closely packed nanoparticle assembly, often with mechanical robustness.[7−11] While the mechanical stability of EPD films over conventional film deposition has been previously demonstrated,[9] little is known about the electronic properties of the films deposited via EPD.

Copper sulfide is a p-type semiconductor material that has generated a great deal of interest due to its potential use in optoelectronic applications. While several methods such as physical deposition methods (evaporation and sputtering),[12] pulsed chemical vapor deposition,[13] and chemical bath deposition methods[14−16] have been used to deposit $Cu_{2-x}S$ films, a facile method suitable for large-scale applications is desirable. Hence, a simple and robust method for solution-based processing of conducting $Cu_{2-x}S$ films is important. In this work, we utilize EPD as an alternate method for depositing conducting copper sulfide nanoparticle films, and we study the effect of deposition methods on electronic transport properties of EPD and spin-cast $Cu_{2-x}S$ films. Our room-temperature method for realizing highly conductive $Cu_{2-x}S$ nanoparticle films involves chemical treatment of as-deposited films with ammonium sulfide—a process that replaces the bulky surfactant ligands with metal-sulfide bonds—transforming the as-deposited insulating films into highly conducting films. When we compare the electronic properties of copper sulfide nanoparticle-based films deposited via electrophoretic deposition and spin-casting, we find that spin-casting can yield films with high conductivities (5.7 $S \cdot cm^{-1}$) and mobilities (4.3 $cm^2 V^{-1} s^{-1}$), and that the EPD films consistently have an order of magnitude higher conductivity (up to 75 $S \cdot cm^{-1}$) than the spin-cast films. We believe this could pave the way for new methods of room-temperature processing of nanoparticles for applications such as printable electronics.

EXPERIMENTAL SECTION

Overview of Experimental Procedures. Our experimental plan is summarized in the schematic of Figure 1a, showing colloidal $Cu_{2-x}S$ nanoparticles utilized as building blocks for the fabrication of nanoparticle films via spin-casting and electrophoretic deposition. The copper sulfide nanoparticles shown in Figure 1b were synthesized in batch to ensure uniformity between multiple devices.[17] In preparation for film deposition the nanoparticles are redispersed in hexanes, cleaned, and filtered through 0.2 μm polyvinylidene fluoride (PVDF) membranes. The nanoparticles are then deposited by spin-casting or EPD onto the substrates, and the electronic properties of the prepared films are studied by performing resistivity, Hall effect, and field effect transistor (FET) measurements. Different substrates and substrate preparations are used for the Hall and FET measurements to match the experimental needs of each characterization method. For the resistivity and Hall measurements, Cr/Au (5 nm/90 nm) electrodes are deposited on borofloat glass and doped-Si/SiO_2 substrates via electron beam evaporation such that after nanoparticle deposition, the films could be manually patterned into 5 mm squares with 200 μm squares of gold contacts at the edges of the film. The FET devices consist of doped-Si/SiO_2/Cr/Au (500 μm/300 nm/5 nm/100 nm) stacks to form a bottom-gate and bottom-contact transistor once the nanoparticle film is deposited. The substrates (both FET and Hall) used for spin-casting were cleaned in isopropanol, acetone, and methanol and vapor primed with hexamethyldisilazane (HMDS) prior to film deposition. For the spin-cast films, ~50 μL of 5 mg/mL of $Cu_{2-x}S$ nanoparticles in hexanes are deposited for 30 s at 2000 rpm. This spin-casting condition is selected after characterizing the properties of films (conductivity and film homogeneity) obtained from varying spin parameters, using primed and unprimed substrates, and varying solution concentration. The EPD of the copper sulfide

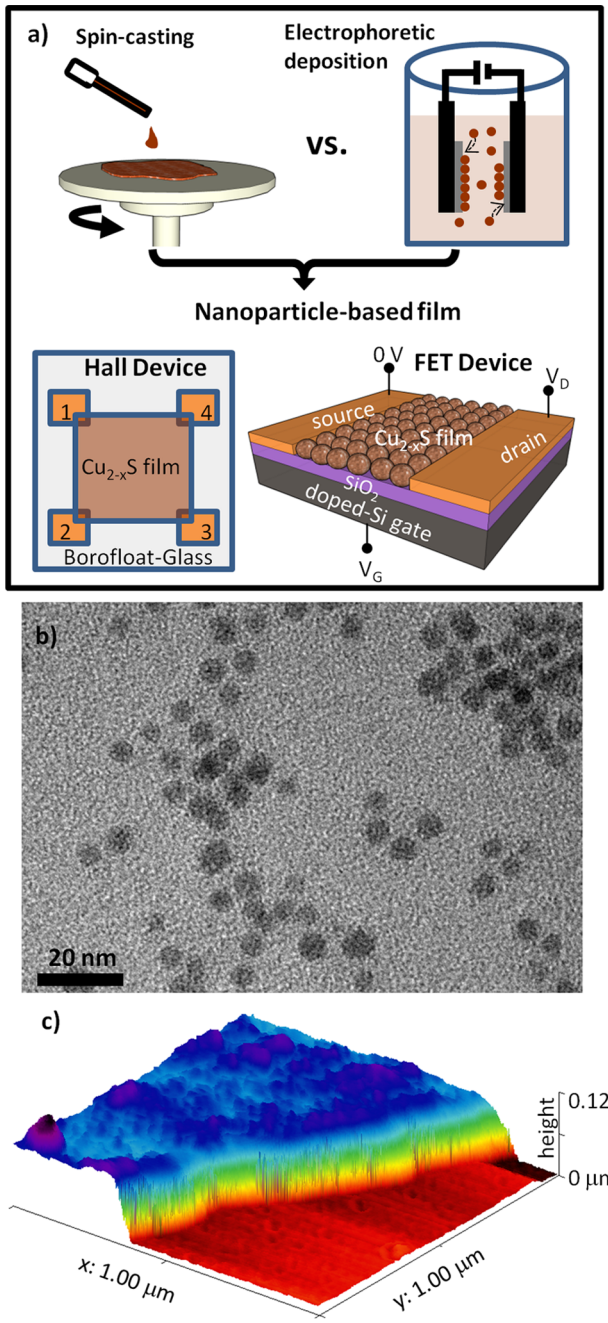

Figure 1. (a) Schematic depiction of experimental plan to study electronic transport in EPD and spin-cast copper sulfide films. (b) TEM of starting copper sulfide nanoparticles with average particle size of 5 nm. (c) AFM height image showing a step in height between the film and regions from which the films have been cleaned, revealing film thickness.

films is carried out by applying a voltages (up to ~600 V) for up to 15 min between two conducting electrodes arranged in a parallel plate capacitor configuration and immersed in a colloidal solution of copper sulfide nanoparticle dispersed in hexanes, as shown in Figure 1a. Particles are attracted to the electrodes via Coulombic interaction. The spacing between the electrodes is ~3 mm, and with hexane having a dielectric constant of ~1.9, the effective electric field for film deposition is ~1050 V/cm. The particles are deposited onto the positive electrode, suggesting our particles are predominantly negatively charged. (See Supporting Information for further details on experimental procedures.)

Optimal Nanoparticle Film Deposition Conditions. Film deposition conditions are optimized to obtain conducting films (>100 nm thickness) in a reproducible manner. The optimal EPD and spin-cast conditions are characterized to ensure that the measured films are of identical thicknesses, as conductivity of the films often exhibit thickness dependent behavior. Ensuring that the film thickness obtained from EPD and spin-casting are identical often requires multiple deposition cycles. Three EPD and ten spin-cast deposition cycles were usually carried out to obtain identical thicknesses of ~120 nm. The film thicknesses are determined using an atomic force microscope (AFM) after cleaning a region of the films with a swab tip soaked in hexanes, as shown in Figure 1c. Each deposition cycle consists of spin-casting/EPD of colloidal nanoparticles onto the substrates/devices, followed by an ammonium sulfide $(NH_4)_2S$ ligand replacement step:[18] after each film layer is made by EPD or spin-casting, the substrate is immersed in a 4 mM $(NH_4)_2S$/methanol solution for 30 s, rinsed in methanol for 30 s, and dried in ambient temperature. The ammonium sulfide ligand replacement strips off the organic ligands and replaces them with sulfide anions, resulting in a metal−sulfur terminated nanoparticle surface.[18] With the removal of the bulky organic groups, the nanoparticles are also brought together in intimate contact. Both these effects (metal−sulfur surface and inorganic connections between nanoparticles) increases interparticle coupling and enhances charge transport. This step is critical for obtaining conductive films; without the ammonium sulfide treatment, the films are insulating (Supporting Information).

RESULTS AND DISCUSSION

Characterization of the colloidal nanoparticle building blocks by transmission electron microscopy (TEM) and the initial film by X-ray diffraction (XRD) show the nanoparticles having an average size of ~5 nm and matching the XRD pattern for copper sulfide (Figures 1b and 2a). The XRD pattern (Figure 2a) can be most closely compared to three different phases of copper sulfide $Cu_{2-x}S$: low Chalcocite, $x \approx 0$; Djurleite, $x = 0.06$; and Roxbyite, $x = 0.19$. Cu_2S has been shown to be an intrinsic semiconductor,[12,19] whereas the $Cu_{1.94}S$ and $Cu_{1.81}S$ are p-type semiconductors due to the presence of copper vacancies.[20−24] The XRD pattern of our measured samples match the Djurleite phase most closely; hence, a p-type semiconducting behavior is expected. However, we note that the exact phase of $Cu_{2-x}S$ has been known to be difficult to distinguish using XRD patterns alone, as mixed phases and transformation between phases is common.[16,21,25,26] After the ammonium sulfide surface underwent ligand treatment, we observe no changes in the XRD patterns, and Scherrer analysis of the XRD peaks indicates a crystal size of ~4.8 nm both before and after treatment (Figure 2a), indicating that the particles have not sintered into larger grains and that they have not disintegrated into smaller crystals. The ammonium sulfide treatment used in preparing these films has previously been shown to increase interparticle coupling.[18] TEM images of samples scraped off the EPD films (Figure 2b,c; also see Figures S1 and S5, Supporting Information, for post-ammonium sulfide treatment spin-cast films) suggest that the nanoparticles in the films have not sintered together from the ammonium sulfide treatment but have formed a closely packed network of nanoparticles inorganically connected, as was seen in work by Zhang et al.[18] Preliminary analysis of film porosity also suggests that EPD films are better packed than spin-cast films (See Figures S2, S4, and S5, Supporting Information). Hence, EPD films should have better interparticle coupling.

The stoichiometry and composition of the EPD and spin-cast films before and after the ammonium sulfide treatments are characterized with X-ray Photoelectron Spectroscopy (XPS).

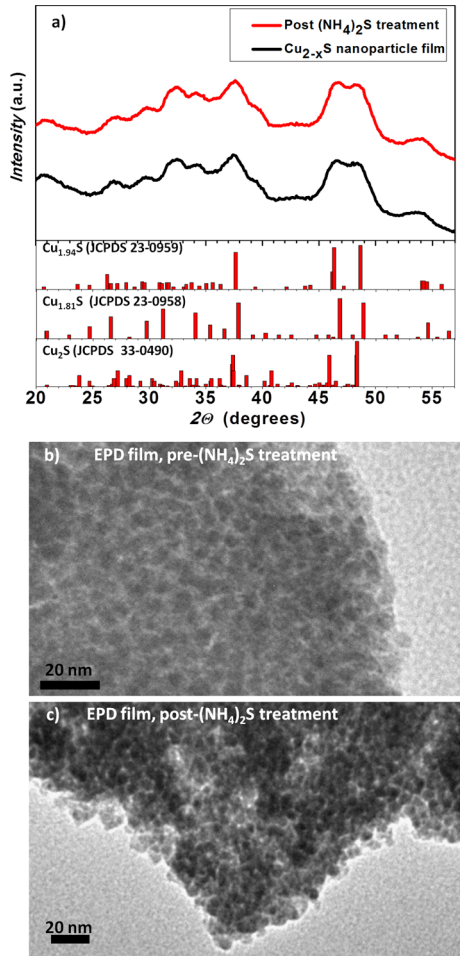

Figure 2. (a) XRD pattern of the copper sulfide film before and after ammonium sulfide treatment compared to the Djurleite $Cu_{1.94}S$ (JCPD 23-0959), Roxbyite $Cu_{1.81}S$ (JCPDS 23-0958), and low-chalcocite Cu_2S (JCPDS 33-0490) phases of copper sulfide. A close match to the Djurleite is observed, indicating the presence of copper vacancies. (b) TEM of $Cu_{2-x}S$ nanoparticles scraped off of EPD films without ammonium sulfide treatment. The films are insulating without ammonium sulfide treatment. (c) TEM of $Cu_{2-x}S$ nanoparticles scraped off of EPD films treated with ammonium sulfide. These films have conductivities as high as 75 $S \cdot cm^{-1}$ at room temperature. The particles are scraped off of films made by three EPD cycles.

Figures S6 and S7 (Supporting Information) show XPS survey scans of spin-cast and EPD-films before and after ammonium sulfide treatment. All XPS spectra are calibrated with the binding energy of the C 1s peak at 284.8 eV and the films were deposited on a doped-Si/SiO_2 substrate. The atomic percentages of the constituent elements are summarized in Table S1 (Supporting Information). The Cu 2p, S 2p, O 1s, C 1s, N 1s, and Si 2 p peaks are used for calculating the atomic percentages. The ratio of Cu/S before the ammonium sulfide treatment for both spin-cast and EPD films is close to 2:1, as expected for $Cu_{2-x}S$. However, due to the presence of a significant amount of C, O, and Si, the stoichiometry information obtained for $Cu_{2-x}S$ from XPS data is not exact. The high-resolution XPS spectra of C 1s in Figures S8 and S9 (Supporting Information) indicate a reduction in carbon content after the ammonium sulfide treatment. After the ammonium sulfide treatment, the ratio of the atomic percentages of Cu/S films is ~1:1. This increase in sulfur

content, in addition to the decrease in C and N peaks, is attributed to the removal of organic ligands and replacement with sulfide anions. The absence of N peaks after treatment also indicates that no inorganic ligands (e.g., $(NH_4)_2S$ or $(NH_4)S^-$) or ammonium or ammonia moieties remain after treatment. These results—increase in sulfur, the lack of nitrogen signal, and the decrease in carbon—are all consistent with our previous work and extensive characterization of this ligand removal process.[18]

From the high-resolution scans of Cu 2p and S 2p in Figure 3, the chemical state of copper and sulfur in the films are

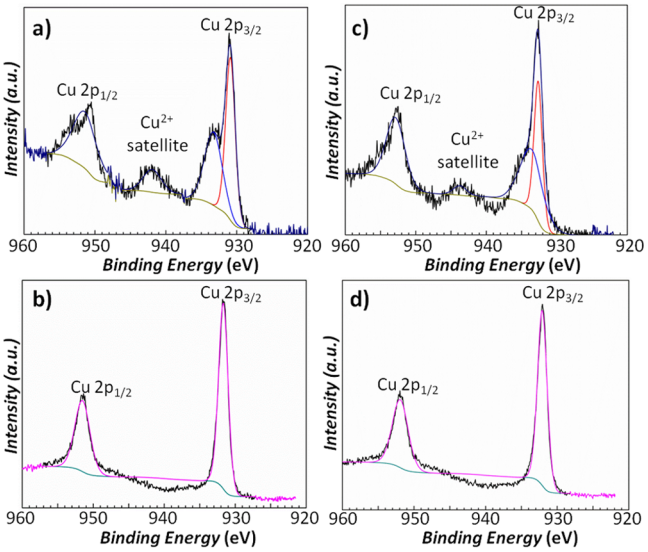

Figure 3. High-resolution XPS scan of the Cu 2p region for spin-cast films (a) before ammonium sulfide treatment and (b) after ammonium sulfide treatment and for EPD film (c) before ammonium sulfide treatment and (d) after ammonium sulfide treatment. The Cu $2p_{3/2}$ peaks in a and c indicate a shift to higher binding energy, a consequence of oxidation. Satellite peaks (Cu^{2+}) at ~943 eV observed in panels a and c are not observed in panels b and d. See Figure S10 (Supporting Information) for corresponding high-resolution scans for the S 2p region.

further assessed. The binding energies of Cu $2p_{3/2}$ and Cu $2p_{1/2}$ are centered at 932.6 and 952.6 eV respectively, indicating a monovalent state of copper (Cu^+) as expected in Cu_2S. In addition, the presence of the Cu $L_3M_{4,5}M_{4,5}$ Auger transition with kinetic energy of 918.5 eV (showing up at binding energy ~568 eV on the survey scans) further suggests a Cu^+ state.[27] The satellite peaks that appear at 943.7 eV in the Cu 2p high-resolution scans before ammonium sulfide treatment in Figure 3a,c are due to oxidation. The S 2p spectra in Figure S10 (Supporting Information) shows a doublet species with binding energies of 162.7 and 163.9 eV corresponding to S $2p_{3/2}$ and S $2p_{1/2}$, respectively. These peaks are indicative of a Cu−S bond formation.[27] While the exact stoichiometry of the $Cu_{2-x}S$ films is difficult to determine because excess S from the processing can produce misleading values, the XPS and XRD results infer that our films are $Cu_{2-x}S$.

Hall effect measurements of the carrier concentration, carrier type, and mobility reveal that the spin-cast copper sulfide films are highly conducting. Colloidal nanoparticles are spin-cast onto the devices for Hall measurements (Figure 1a). The substrates (in our case, glass) for Hall measurements should be nonconducting, on which EPD cannot be performed. All electrical measurements were done in a Physical Property Measurement System (PPMS, Quantum Design). Sheet resistance was measured using the standard van der Pauw approach by determining resistance $R_{14,23}$, the resistance obtained by applying a DC current (I_{14}) through gold contacts 1 and 4 and measuring the voltage (V_{23}) that develops between gold contacts 2 and 3. By swapping the contact points for current injection and voltage measurements, we observe identical resistance values and conclude that the films are of uniform thickness and suitable for Hall measurements. The sheet resistance is expressed as $R_s = \pi R_{14,23}/(\ln 2)$.[28] For Hall effect measurements, we measure the voltage between contacts 2 and 4, while the current is applied between contacts 1 and 3 in the presence of a magnetic field.

In Figure 4, the room-temperature magnetic-field-dependent Hall voltage V_H, measured for two spin-cast films (spin-on-glass

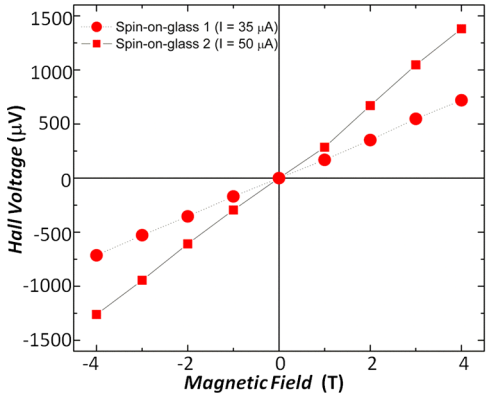

Figure 4. Hall effect measurements for two spin-cast films on glass substrates. Films are treated with ammonium sulfide. The Hall voltage is determined for varying magnetic field (−4 to 4 T). Polarity of the Hall voltage indicates the $Cu_{2-x}S$ are p-type semiconducting.

1 and **2**) is shown. These samples were prepared identically. The film thicknesses, d, measured from profilometry and AFM of the two samples **1** and **2** is determined to be 112 and 120 nm, respectively. The positive polarity at positive magnetic fields (0 to 4 T) of V_H is indicative of a p-type material, which is commonly reported for copper sulfide films with copper vacancies.[12,14,15,21,29] To ensure measurement accuracy, the polarity of the magnetic field is reversed. After magnetic field reversal, we observe that the polarity of V_H changes, but the magnitude remains approximately the same. This implies an accurate measurement of Hall voltage. We determine the conductivity ($\sigma = 1/R_s d$,) of spin-on-glass samples **1** and **2** to be 5.74 and 5.44 S·cm^{-1}, respectively. We determine the Hall carrier concentration n_H and Hall mobility μ_H using the expressions $\sigma = n_H e \mu_H$ and $V_H = ((IB)/(n_H e d))$, where e is the elementary charge (1.602×10^{-19} C), I is the applied current, and B is the applied magnetic field. These results are summarized in Table 1. Compared to transistor-based measurements, Hall measurements have the advantage of studying the intrinsic charge transport in nanoparticle-based films independent of charge trapping effects.[28,30] Our Hall measurements result in Carrier concentrations of ~10^{19} cm^{-3} and Hall mobilities of ~3.3 and 4.3 cm^2 V^{-1} s^{-1} for our spin-cast $Cu_{2-x}S$ nanoparticle films **1** and **2**, respectively. Because our films are insulating before the ligand replacement step, we attribute these high conductivities to the post-deposition ammonium sulfide treatment, which increases interparticle

Table 1. Hall Effect Measurements on Spin-Cast Nanoparticle-Based Films

spin-on-glass films	slope (V/T)	film thickness (nm)	conductivity ($S \cdot cm^{-1}$)	carrier density (cm^{-3})	Hall mobility ($cm^2\ V^{-1}\ s^{-1}$)
1	1.79×10^{-4}	112	5.74	1.09×10^{19}	3.28
2	3.28×10^{-4}	120	5.44	7.93×10^{18}	4.28

coupling. Recent results have also shown conductivity enhancements in $CuInSe_2$ films with virtually bare nanoparticle surfaces after ligand exchange with 1-ethyl-5-thioterazole.[31]

The high conductivities and carrier concentrations of our films are comparable to values previously obtained from low-chalcocite ($Cu_{1.999}S$ and $Cu_{1.995}S$) copper sulfide films prepared by thermal evaporation (~1 μm thick) and RF sputtering techniques (0.1−0.5 μm thick): $Cu_{1.999}S$ (7 $S \cdot cm^{-1}$ and 1.5×10^{19} cm^{-3}) and $Cu_{1.995}S$ (35 $S \cdot cm^{-1}$ and 10^{20} cm^{-3}).[12] Even higher conductivities have been reported for anilite phase ($Cu_{1.75}S$) copper sulfide films,[29] although we note that (1) copper sulfides are typically p-type from copper vacancies, with more copper vacancies generally leading to higher conductivity, (2) XRD from Figure 2a suggests that our measured films are of the Djurleite phase ($Cu_{1.94}S-Cu_{1.96}S$), which has fewer copper vacancies than the anilite phase and more copper vacancies than the low-chalcocite phase, (3) the anilite phase is expected to have higher conductivity than our Djurleite films, as there are more copper vacancies in anilite, and (4) our films are made from nanosize grains without thermal annealing and should not be expected to compete with bulk; however, our results show comparable values to thermally processed bulk films. Thus, our measured values of conductivities are remarkably high. When compared to copper sulfide films prepared by pulsed chemical vapor deposition of identical thickness (~120 nm) and stoichiometry (between $Cu_{1.9}S$ to Cu_2S), our nanoparticle-based films show better or identical conductivities.[13] In Table S2 (Supporting Information), we summarize the electrical conductivities of some copper sulfide films previously reported, and we note their stoichiometry and method of determination, synthesis and deposition methods, and film thicknesses. Although the results are widely ranging,[12−16,29,32] we can infer that increasing copper vacancies suggest higher conductivities, that annealed films have higher conductivities than unannealed films, and that our solution-processed nanoparticle films perform on par with some of the physically deposited films, even though our nanoparticles have not been annealed.

It is interesting to note that a low-cost solution-based process is able to realize highly conducting films comparable to bulk deposition methods without annealing. Our films have hole mobilities that are 1−4 orders of magnitude higher than hole mobilities previously reported for heat treated nanoparticle films of HgTe, InSb, PbS, PbTe, and PbSe.[33] Our films also have 1−7 orders of magnitude higher conductivity than those of some previously reported metallic nanoparticles of Au, $CoPt_3$, Ag, Pb, Co, and Pd.[34] Hence, our films are applicable as p-type conducting films and as conducting electrodes in an all-nanoparticle based device. However, we note that it is difficult to compare different material systems exactly. Such highly conductive nanoparticle-based films made without thermal annealing have also been recently reported for silver nanoparticles.[35] These silver films are metallic in nature, while our $Cu_{2-x}S$ films are p-type semiconducting; hence, our films are more suitable active materials for electronic and optoelectronic applications. In addition, although silver nanoparticle-based films could be used for device electrodes, $Cu_{2-x}S$ films with high conductivities could also be used as electrodes with the added advantage of transparency, although the transparency will be dependent on film thickness.[29]

The effect of film deposition methods on the electronic properties of these highly conducting $Cu_{2-x}S$ are analyzed through temperature-dependent conductivity measurements on films (made via EPD and spin-casting) of identical thicknesses deposited on doped-Si/SiO_2 substrates with Au contact pads. The device geometry is similar to those used for the Hall measurements above, with the exception of a doped-Si/SiO_2 substrate in place of the glass substrate. EPD works for these substrates because the doped silicon is conductive. In addition, we measured the temperature dependence of the conductivity of spin-cast films (spin-on-glass **1** and **2**) that were used for Hall effect measurements. All the electrical measurements are carried out in the PPMS, and Ohmic contacts are ensured through wire-bonding. Conductivity is measured following the van der Pauw method described above, and film thicknesses are obtained from profilometry and AFM measurements. In Figure 5a, we show the temperature-dependent conductivity of $Cu_{2-x}S$ nanoparticle films formed by EPD (blue symbols) and spin-casting (red symbols), between 25 and 300 K. The plots with open red circles and open red diamonds are measurements of films spin-cast onto glass substrates, while the plot with solid red circles is from a film spin-cast onto doped-Si/SiO_2 substrates. Clearly, the effect of the substrate type on conductivity measurements is not discernible. Slight variations in the properties of EPD films between runs are known to result from uncontrolled experimental conditions, such as humidity and temperature.[7,8]

On the basis of the results in Figure 5a, two points are worth noting: (1) EPD films have an order of magnitude higher conductivity than spin-cast films, and (2) the conductivity of the films decreases with decreasing temperature. At room temperature, the highest conductivity of all the measured EPD films is ~75 $S \cdot cm^{-1}$, while the highest conductivity from the spin-cast films is 5.7 $S \cdot cm^{-1}$. This corresponds to resistivities of ~13.6 m$\Omega \cdot$cm and ~174 m$\Omega \cdot$cm, respectively. We attribute this order of magnitude enhancement in conductivity seen in EPD films to the close-packing of the nanoparticles, as shown in Figure S1 (Supporting Information). EPD is suggested to produce closely packed films in an energetically favored assembly,[36] whereas spin-cast films are prone to disorder.[7] These temperature-dependent studies further confirm our earlier assertion that EPD films produce better conducting films than spin-cast films. We can infer from such conductivity trends that EPD films will likely have higher carrier mobilities than spin-cast films. We note that while the ammonium sulfide treatment may introduce some impurities that could potentially dope the films, the EPD and spin-cast films are subjected to identical ammonium sulfide treatment processes.

To clarify the conductivity effects, it is necessary to consider the pore volume of the films.[37] The improvement in conductivity of EPD over spin-casting can be a result of higher packing order or better interlinking of the nanoparticles in the film. SEM images (Figures S1 and S4, Supporting Information) indicate that the EPD films are better packed than spin-cast

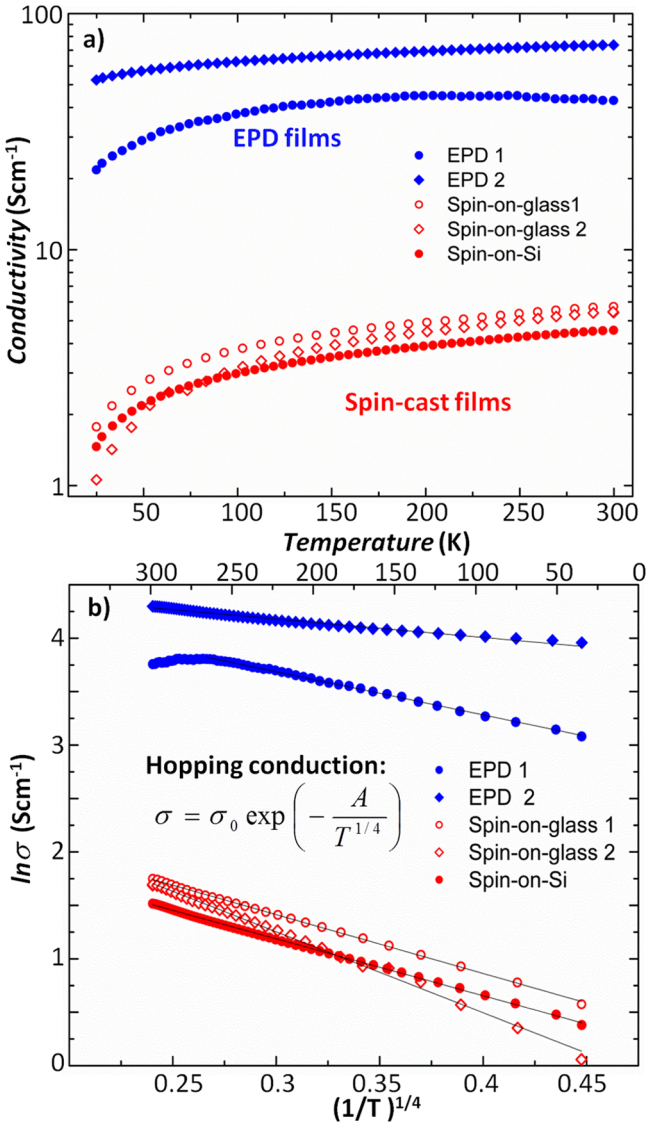

Figure 5. (a) Temperature-dependent electrical conductivity measurements of EPD and spin-cast films from 25 to 300 K showing a decrease in conductivity with deceasing temperature. EPD films show an order of magnitude enhancement in conductivity. (b) Semilog plot of conductivity (ln σ) vs $(1/T)^{1/4}$ shows variable-range hopping (VRH) conduction. The black solid lines are fits of the conductivity using Mott-VRH with one-fourth power−temperature dependence. The data is best fit to a Mott-VRH (Table S4, Supporting Information).

films. To better assess the average porosity, we measure the mass (before and after deposition) and thickness of the EPD and spin-cast films deposited on a 15 × 15 mm^2 silicon substrate and calculate the film density. By assuming a bulk density of 5.6 g/cm^3 for Cu_2S, we estimate the percentage porosity and the solid fraction of the films (Table S3, Supporting Information). EPD films have ∼38% film porosity and 0.62 solid fraction, while spin-cast films have ∼57% film porosity and 0.43 solid fraction, indicating a higher packing fraction for the EPD films. These calculated values are in good agreement with the 2D solid fraction ("% area") obtained from image-processed SEM images in Figure S4 (solid fraction of 0.63 for EPD and 0.40 for spin-cast; Supporting Information). The experimentally measured conductivity ($\sigma_{measured}$) should be related to the interlinking conductivity (σ_{IL}) of the nanoparticles and the solid fraction (S_f) of the films by $\sigma_{measured} = \sigma_{IL}S_f$. To understand this effect, we rescaled the temperature-dependent conductivity of the films shown in Figure 5a to express conductivity as the interlinking conductivity ($\sigma_{IL} = \sigma_{measured}/S_f$), as shown in Figure S11 (Supporting Information). Despite this normalizing for solid fraction, the EPD films still show an order of magnitude increase in conductivity compared to the spin-cast films. The results of this analysis implies that while the EPD films are less porous (denser) than spin-cast films, porosity alone does not account for the order of magnitude difference in conductivity. We can conclude from this study that the interlinking between particles is enhanced in EPD processing.

Analysis of the carrier transport mechanism from the temperature-dependent conductivities of the films reveals a hopping conduction mechanism for charge transport (Figure 5b). The trend shows a decrease in conductivity (ln σ) with decreasing temperature, which is typical for semiconductors where thermally activated hopping—the process in which a charge carrier in a localized state moves to another state via energy it receives from a phonon—is prominent.[38] The hopping process extends beyond nearest neighbors with the further-distance hops resulting from smaller energy barriers. This process is counterbalanced by a decreasing tunneling probability over large distances, such that the conductivity is of the form $\sigma = \sigma_0 \exp(-A/T^n)$,[38−40] where A is a constant proportional to the activation energy and hopping probability. The power law (n) dependence of the temperature in the conductivity equation is reported as 1 or $^1/_2$ for nearest-neighbor hopping (also thermally activated hopping) or Efros−Shklovskii VRH, respectively.[40−42] However, our data are best fit with a power of $^1/_4$, suggesting a Mott VRH mechanism (Table S4, Supporting Information).[38,42] The linear dependence of ln σ versus $T^{-1/4}$ from 25 to ∼270 K in the spin-cast films and the EPD films in Figure 5b is therefore indicative of variable-range hopping conduction in both films. While previous work showed a transition temperature at which conduction changes from VRH to nearest-neighbor hopping,[43] our results do not exhibit any such transition in hopping mechanism, which is a similar conclusion found by Houtepen et al. for a $T^{-2/3}$ conductivity dependence in ZnO nanoparticles.[44] The parameters A and σ_0 in the conductivity equation are extracted for Mott-VRH and shown in Table 2. The pre-

Table 2. Linear Fits of Conductivity to Mott Variable Range Hopping Equation

	A ($K^{1/4}$)	σ_0 ($S{\cdot}cm^{-1}$)
EPD 1	4.04	134.04
EPD 2	1.74	110.04
spin (glass) 1	5.51	21.45
spin (glass) 2	7.57	33.94
spin (Si)	5.32	16.19

exponential factor σ_0, which is about an order of magnitude higher in the EPD films than in the spin-cast films, is inversely proportional to the lattice spacing,[38] further suggesting that better interparticle coupling is responsible for the enhanced conductivity in EPD films. Between 270 and 300 K, we observe that the conductivity in the EPD-1 film begins to deviate subtly from the expected hopping behavior, and, in fact, conductivity begins to decrease with increasing temperature. While the source of the deviation is not fully clear, such a trend of decreasing conductivity with increasing temperature has been

observed in other studies on nanoparticle films where metal-like transport is suggested based on field-effect mobility measurements.[28,45,46]

The temperature stability of the films is studied by extending the temperature range to 400 K (the maximum temperature of the PPMS). In Figure S12, Supporting Information, we show the resistivity data for two films made by EPD and spin-casting. We cycled the temperature from 300 to 25 K, and then from 25 to 400 K. For both film types, cycling from 25 to 300 K results in an increase in resistivity with a decrease in temperature; however, when cycling from 25 to 400 K, a sharp and irreversible drop in resistivity (increased conductivity) is observed in the EPD and spin-cast film at ∼350 K and ∼380 K, respectively. The drop in resistivity suggests that the films are likely sintering at these higher temperatures. It is interesting to note that the EPD films sinter at lower temperatures than the spin-cast films. This is possibly due to the tighter packing of the EPD films over the spin-cast films. In addition, we note that a recent study demonstrated irreversible thermal doping in Cu_2S nanoparticle films above 350 K, and this may provide an alternative explanation.[22]

We also assessed the light-sensitivity of the performance by measuring EPD and spin-cast films under 150 W illumination (Micro-Lite FL2000 High Intensity Fiber Optic Illuminator). For this study, we varied the electrode spacing and obtained the current-voltage characteristics of the films with four-wire resistance measurements. We find negligible light sensitivity in all cases. (See Supporting Information Figure S13 for discussions on aging the films in ambient conditions and Figures S14 and S15 for data on light stability.)

In Figure 6, we show the output and transfer characteristics of FET devices. The transistor geometry is bottom-gate bottom-contact, with the nanoparticles deposited onto the source and drain electrodes via EPD and spin-casting (schematic of construction shown in Figure 1a). The film thicknesses of the EPD and spin-cast films are ∼350 nm and ∼70 nm thick, respectively. The resulting transistor channel is 2.5 μm wide and 1 mm long. At gate voltage V_{GS} = 0 V, a substantial drain-to-source current (I_{DS}) of ∼0.96 mA is measured at a drain-to-source voltage V_{DS} = 4 V for EPD films, whereas at the same V_{DS} and V_{GS}, the drain current in the spin-cast films is ∼4.2 μA. Because conduction in FETs occur mostly via the surface channel, the difference in thickness cannot account for 2 orders of magnitude difference in current levels; hence, the higher current levels obtained from the EPD films further suggests that EPD films consistently form more conducting films than spin-cast films. The I_{DS}−V_{DS} graph is shown in logarithm scale in order to display the differences between the EPD and spin-cast data on a single plot. Due to the 2 orders of magnitude difference in I_{DS} between the EPD and spin-cast films, the features of the spin-cast data are suppressed when plotted on a traditional linear-scale (Figure S16, Supporting Information). I_{DS} is slightly increased by changing the gate voltage from zero to negative values (−10 and −20 V) for both EPD and spin-cast films, which is expected for a p-type semiconducting material, although the gate modulation is weak and no saturation occurs. Because the $Cu_{2-x}S$ films obtained from EPD and spin-casting are conducting, utilizing them in a FET-geometry as channel material would imply a depletion-mode operation for such transistor. Transfer characteristics (I_{DS}−V_{GS} plots at V_{DS} = 5 V) of FETs made from both EPD and spin-cast films shown in Figure 6b, depict no rectification; however, qualitative assessment of the plots indicate that the gate modulation is minimal and that the drain-source current level decreases by using positive gate voltages. The change in slope observed in the I_{DS}−V_{GS} plot of the EPD film near V_{GS} = 0 V, which is not seen for the spin-cast films, is likely due to carrier depletion in the channel with positive gate voltages; however, the influence of charge trapping sites, which may be different for each film type might result in the disparity. Further studies on charge trapping mechanisms might provide better clarifications. From the I_{DS}−V_{GS} plot, we calculated field-effect mobilities of 1.12 and 0.0087 $cm^2\ V^{-1}\ s^{-1}$ for the EPD and spin-cast films, respectively. We note that the field-effect mobility of the spin-cast sample is lower than that obtained from Hall effect mobilities in Table 1. Although, FET measurements have been typically used to characterize the electronic properties of nanoparticle films, the results are strongly affected by charge trapping.[28]

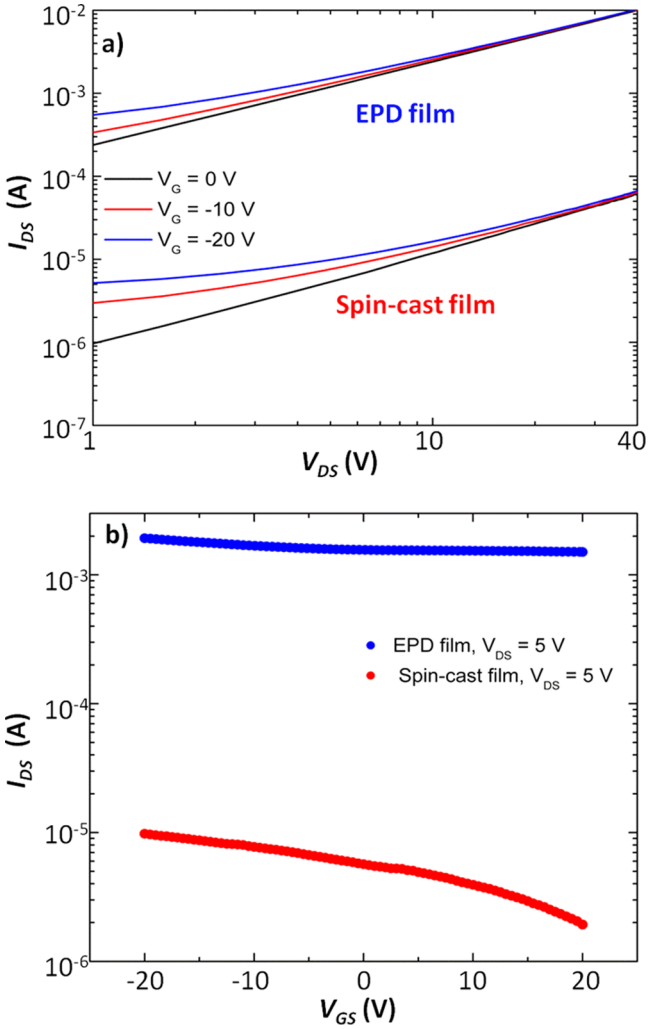

Figure 6. FET measurements of EPD and spin-cast films. (a) Log−log plot of drain-source current as a function of drain-source voltage (FET output characteristics). The plot shows minimal gate modulation and no saturation for both films. Channel width, 1 mm; channel length, 2.5 μm. Slight increase in drain current with negative gate voltages suggests a p-type channel. (b) Semilog plots of drain-source current as a function of gate voltage (FET transfer characteristics) at a constant V_{DS} of 5 V. EPD films conduct higher drain currents than spin-cast films. FET mobilites extracted from plots in panel b are 1.12 and 0.0087 $cm^2\ V^{-1}\ s^{-1}$ for EPD and spin-cast films, respectively.

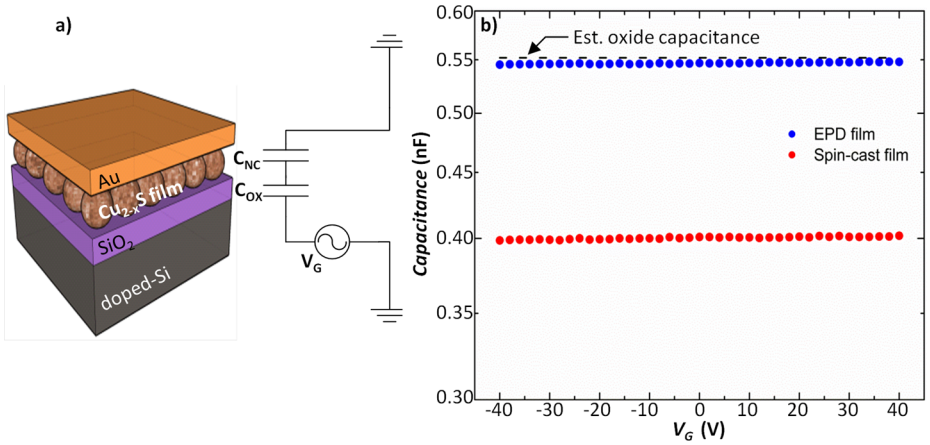

Figure 7. (a) Schematic of the of metal (Au)−semiconductor (copper sulfide)−insulator (silicon oxide)−metal (doped-Si) (MSIM) capacitors fabricated with EPD and spin-cast films. Also shown is the equivalent capacitance of the MSIM structure, which is a series connection of oxide (C_{OX}) and nanoparticle film capacitance (C_{NP}). (b) High-frequency (100 kHz) capacitance−voltage (C−V) measurements of the MSIM capacitor in panel a. Estimated oxide capacitance assumes a dielectric constant of 3.9 and thickness of ∼300 nm. Area is ∼4.8 mm^2.

Capacitance−voltage (C−V) measurements of EPD and spin-cast films reveal that the films are highly doped, as their capacitance shows no voltage dependence. We fabricate metal (Au)−semiconductor (copper sulfide)−insulator (silicon oxide)−metal (doped-Si) (MSIM) capacitors (Figure 7a) and measured the equivalent capacitance C_{EQ} sweeping gate voltage from −45 to 45 V at 100 kHz with a precision LCR meter (Agilent 4284), as shown in Figure 7b. The equivalent capacitance of the MSIM structures—a series arrangement of oxide capacitance C_{OX} and nanoparticle film capacitance C_{NP}—is shown in Figure 7a. The measured equivalent capacitance $C_{EQ} = (1/C_{OX} + 1/C_{NP})^{-1}$. With increasing film capacitance, C_{EQ} tends toward C_{OX}. The estimated oxide capacitance C_{OX} is ∼0.552 nF as depicted in Figure 7b (assuming a dielectric constant of 3.9 for silicon oxide, area of 4.88 mm^2, and an oxide thickness of 300 nm.) Varying the gate voltage has negligible effect on the equivalent capacitance measured for both EPD (0.545 nF) and spin-cast films (0.4 nF), which further supports the minimal gate modulation seen in the output characteristics in Figure 6a. These results, however, further support our assertion that more mobile charges are accumulated in EPD films than in spin-cast films; hence, the EPD films will have higher drain-to-source currents, as found in the FET measurements above. The constant capacitance with gate voltage confirms that the $Cu_{2-x}S$ films obtained from both EPD and spin-cast are highly doped. Although it is difficult to quantify the carrier concentration from C−V plots,[47] the Hall effect measurements shown in Figure 4 help to assess the highly doped nature of the films.

CONCLUSION

While the high conductivity observed in these $Cu_{2-x}S$ films does not make them ideal candidates for FET channel materials, they could potentially be utilized as source and drain electrode materials in an all-nanoparticle based transistor, as was recently demonstrated with Ag nanoparticles for the source and drain electrodes.[35] In addition, $Cu_{2-x}S$ films could be employed as highly conducting p-type transparent conducting electrodes.[29] The order of magnitude enhancement in conductivity obtained for our EPD films could be applied to enhance the conductivities of films shown to have high electron mobilities (>10 $cm^2\ V^{-1}\ s^{-1}$) only after heat treatment or chemical doping.[46,48]

In summary, we have shown that ammonium sulfide treatment of insulating $Cu_{2-x}S$ nanoparticle-based films results in highly conducting films comparable to physically deposited thin films. Further, we show that EPD results in an order of magnitude enhancement in conductivity of these $Cu_{2-x}S$ films over spin-casting. The increase in conductivity is attributed to better interparticle coupling in the EPD films. The result of this study presents a scalable route to producing highly electrically conductive solution-processed films for electronic and opto-electronic applications.

ASSOCIATED CONTENT

Supporting Information

Experimental methods, percentage area estimations, XPS film composition, time and light stability data, figures, tables. This material is available free of charge via the Internet at http://pubs.acs.org.

AUTHOR INFORMATION

Corresponding Author

*E-mail: rdr82@cornell.edu. Web site: http://robinson.mse.cornell.edu.

Notes

The authors declare no competing financial interest.

ACKNOWLEDGMENTS

We thank M. G. Spencer, J. Shu, S. Kriske, and K. Whitham for helpful discussions. The work was supported in part by the National Science Foundation under Agreement No. DMR-1149036, and in part by the Energy Materials Center at Cornell (EMC^2), an Energy Frontier Research Center funded by the U.S. Department of Energy, Office of Science, Office of Basic Energy Science under Award Number DE-SC0001086. O.O.O. was fully supported through the NSF (DMR-1149036). This work made use of the Cornell Center for Materials Research Shared Facilities, which are supported through the NSF MRSEC program (DMR-1120296). This publication is based on work supported in part by Award No. KUS-C1-018-02, made by King Abdullah University of Science and Technology (KAUST). Device fabrication was performed at the Cornell

Nanoscale Facility, a member of the National Nanotechnology Infrastructure Network, which is supported by the National Science Foundation (Grant ECS-0335765).

REFERENCES

(1) Talapin, D. V.; Murray, C. B. Pbse Nanocrystal Solids for N- and P-Channel Thin Film Field-Effect Transistors. *Science* **2005**, *310*, 86−89.
(2) Gur, I.; Fromer, N. A.; Geier, M. L.; Alivisatos, A. P. Air-Stable All-Inorganic Nanocrystal Solar Cells Processed from Solution. *Science* **2005**, *310*, 462−465.
(3) Coe, S.; Woo, W. K.; Bawendi, M.; Bulovic, V. Electroluminescence from Single Monolayers of Nanocrystals in Molecular Organic Devices. *Nature* **2002**, *420*, 800−3.
(4) Talapin, D. V.; Lee, J.-S.; Kovalenko, M. V.; Shevchenko, E. V. Prospects of Colloidal Nanocrystals for Electronic and Optoelectronic Applications. *Chem. Rev.* **2009**, *110*, 389−458.
(5) Ocier, C. R.; Whitham, K.; Hanrath, T.; Robinson, R. D. Chalcogenidometallate Clusters as Surface Ligands for PbSe Nanocrystal Field-Effect Transistors. *J. Phys. Chem. C* **2014**, *118*, 3377−3385.
(6) Besra, L.; Liu, M. A Review on Fundamentals and Applications of Electrophoretic Deposition (EPD). *Prog. Mater. Sci.* **2007**, *52*, 1−61.
(7) Song, K. W.; Costi, R.; Bulović, V. Electrophoretic Deposition of Cdse/Zns Quantum Dots for Light-Emitting Devices. *Adv. Mater.* **2013**, *25*, 1420−1423.
(8) Islam, M. A.; Xia, Y.; Telesca, D. A.; Steigerwald, M. L.; Herman, I. P. Controlled Electrophoretic Deposition of Smooth and Robust Films of CdSe Nanocrystals. *Chem. Mater.* **2003**, *16*, 49−54.
(9) Ha, D.-H.; Islam, M. A.; Robinson, R. D. Binder-Free and Carbon-Free Nanoparticle Batteries: A Method for Nanoparticle Electrodes without Polymeric Binders or Carbon Black. *Nano Lett.* **2012**, *12*, 5122−5130.
(10) Hasan, S. A.; Kavich, D. W.; Dickerson, J. H. Sacrificial Layer Electrophoretic Deposition of Free-Standing Multilayered Nanoparticle Films. *Chem. Commun.* **2009**, 3723−3725.
(11) Islam, M. A.; Herman, I. P. Electrodeposition of Patterned CdSe Nanocrystal Films Using Thermally Charged Nanocrystals. *Appl. Phys. Lett.* **2002**, *80*, 3823−3825.
(12) Wagner, R.; Wiemhöfer, H. D. Hall Effect and Conductivity in Thin Films of Low Temperature Chalcocite Cu2S at 20 °C as a Function of Stoichiometry. *J. Phys. Chem. Solids* **1983**, *44*, 801−805.
(13) Carbone, I.; Zhou, Q.; Vollbrecht, B.; Yang, L.; Medling, S.; Bezryadina, A.; Bridges, F.; Alers, G. B.; Norman, J. T.; Kinmen, T. Pulsed Chemical Vapor Deposition of Cu_2S into a Porous TiO_2 Matrix. *J. Vac. Sci. Technol., A* **2011**, *29*, 051505.
(14) Grozdanov, I.; Najdoski, M. Optical and Electrical-Properties of Copper Sulfide Films of Variable Composition. *J. Solid State Chem.* **1995**, *114*, 469−475.
(15) Cardoso, J.; GomezDaza, O.; Ixtlilco, L.; Nair, M. T. S.; Nair, P. K. Conductive Copper Sulfide Thin Films on Polyimide Foils. *Semicond. Sci. Technol.* **2001**, *16*, 123−127.
(16) Nair, M. T. S.; Nair, P. K. Chemical Bath Deposition of Cu_xS Thin Films and Their Prospective Large Area Applications. *Semicond. Sci. Technol.* **1989**, *4*, 191.
(17) Zhang, H. T.; Hyun, B. R.; Wise, F. W.; Robinson, R. D. A Generic Method for Rational Scalable Synthesis of Monodisperse Metal Sulfide Nanocrystals. *Nano Lett.* **2012**, *12*, 5856−5860.
(18) Zhang, H. T.; Hu, B.; Sun, L. F.; Hovden, R.; Wise, F. W.; Muller, D. A.; Robinson, R. D. Surfactant Ligand Removal and Rational Fabrication of Inorganically Connected Quantum Dots. *Nano Lett.* **2011**, *11*, 5356−5361.
(19) Liu, X.; Wang, X.; Zhou, B.; Law, W.-C.; Cartwright, A. N.; Swihart, M. T. Size-Controlled Synthesis of $Cu_{2-x}E$ (E = S, Se) Nanocrystals with Strong Tunable near-Infrared Localized Surface Plasmon Resonance and High Conductivity in Thin Films. *Adv. Funct. Mater.* **2013**, *23*, 1256−1264.
(20) Sands, T. D.; Washburn, J.; Gronsky, R. High Resolution Observations of Copper Vacancy Ordering in Chalcocite (Cu_2S) and the Transformation to Djurleite ($Cu_{1.97\ to\ 1.94}S$). *Phys. Status Solidi A* **1982**, *72*, 551−559.
(21) Zhao, Y.; Pan, H.; Lou, Y.; Qiu, X.; Zhu, J.; Burda, C. Plasmonic $Cu_{2-x}S$ Nanocrystals: Optical and Structural Properties of Copper-Deficient Copper(I) Sulfides. *J. Am. Chem. Soc.* **2009**, *131*, 4253−4261.
(22) Bekenstein, Y.; Vinokurov, K.; Keren-Zur, S.; Hadar, I.; Schilt, Y.; Raviv, U.; Millo, O.; Banin, U. Thermal Doping by Vacancy Formation in Copper Sulfide Nanocrystal Arrays. *Nano Lett.* **2014**, *14*, 1349−1353.
(23) Xie, Y.; Riedinger, A.; Prato, M.; Casu, A.; Genovese, A.; Guardia, P.; Sottini, S.; Sangregorio, C.; Miszta, K.; Ghosh, S.; Pellegrino, T.; Manna, L. Copper Sulfide Nanocrystals with Tunable Composition by Reduction of Covellite Nanocrystals with Cu^+ Ions. *J. Am. Chem. Soc.* **2013**, *135*, 17630−17637.
(24) Luther, J. M.; Jain, P. K.; Ewers, T.; Alivisatos, A. P. Localized Surface Plasmon Resonances Arising from Free Carriers in Doped Quantum Dots. *Nat. Mater.* **2011**, *10*, 361−366.
(25) Li, W.; Shavel, A.; Guzman, R.; Rubio-Garcia, J.; Flox, C.; Fan, J.; Cadavid, D.; Ibanez, M.; Arbiol, J.; Morante, J. R.; Cabot, A. Morphology Evolution of $Cu_{2-x}S$ Nanoparticles: From Spheres to Dodecahedrons. *Chem. Commun.* **2011**, *47*, 10332−10334.
(26) Saldanha, P. L.; Brescia, R.; Prato, M.; Li, H.; Povia, M.; Manna, L.; Lesnyak, V. Generalized One-Pot Synthesis of Copper Sulfide, Selenide-Sulfide, and Telluride-Sulfide Nanoparticles. *Chem. Mater.* **2014**, *26*, 1442−1449.
(27) Shan, J.; Pulkkinen, P.; Vainio, U.; Maijala, J.; Merta, J.; Jiang, H.; Serimaa, R.; Kauppinen, E.; Tenhu, H. Synthesis and Characterization of Copper Sulfide Nanocrystallites with Low Sintering Temperatures. *J. Mater. Chem.* **2008**, *18*, 3200−3208.
(28) Jang, J.; Liu, W.; Son, J. S.; Talapin, D. V. Temperature-Dependent Hall and Field-Effect Mobility in Strongly Coupled All-Inorganic Nanocrystal Arrays. *Nano Lett.* **2014**, *14*, 653−662.
(29) Liufu, S.-C.; Chen, L.-D.; Yao, Q.; Huang, F.-Q. In Situ Assembly of Cu_xS Quantum-Dots into Thin Film: A Highly Conductive P-Type Transparent Film. *J. Phys. Chem. C* **2008**, *112*, 12085−12088.
(30) Podzorov, V.; Menard, E.; Rogers, J. A.; Gershenson, M. E. Hall Effect in the Accumulation Layers on the Surface of Organic Semiconductors. *Phys. Rev. Lett.* **2005**, *95*, 226601.
(31) Lauth, J.; Marbach, J.; Meyer, A.; Dogan, S.; Klinke, C.; Kornowski, A.; Weller, H. Virtually Bare Nanocrystal Surfaces: Significantly Enhanced Electrical Transport in $CuInSe_2$ and $CuIn_{1-x}Ga_xSe_2$ Thin Films Upon Ligand Exchange with Thermally Degradable 1-Ethyl-5-thiotetrazole. *Adv. Funct. Mater.* **2014**, *24*, 1081−1088.
(32) Leong, J. Y.; Yee, J. H. Hall Effect in Reactively Sputtered Cu_2S. *Appl. Phys. Lett.* **1979**, *35*, 601−602.
(33) Hetsch, F.; Zhao, N.; Kershaw, S. V.; Rogach, A. L. Quantum Dot Field Effect Transistors. *Mater. Today* **2013**, *16*, 312−325.
(34) Zabet-Khosousi, A.; Dhirani, A. A. Charge Transport in Nanoparticle Assemblies. *Chem. Rev.* **2008**, *108*, 4072−4124.
(35) Fafarman, A. T.; Hong, S.-H.; Oh, S. J.; Caglayan, H.; Ye, X.; Diroll, B. T.; Engheta, N.; Murray, C. B.; Kagan, C. R. Air-Stable, Nanostructured Electronic and Plasmonic Materials from Solution-Processable, Silver Nanocrystal Building Blocks. *ACS Nano* **2014**, *8*, 2746−2754.
(36) Singh, A.; English, N. J.; Ryan, K. M. Highly Ordered Nanorod Assemblies Extending over Device Scale Areas and in Controlled Multilayers by Electrophoretic Deposition. *J. Phys. Chem. B* **2012**, *117*, 1608−1615.
(37) Lyons, P. E.; De, S.; Blighe, F.; Nicolosi, V.; Pereira, L. F. C.; Ferreira, M. S.; Coleman, J. N. The Relationship between Network Morphology and Conductivity in Nanotube Films. *J. Appl. Phys.* **2008**, *104*, 044302.
(38) Mott, N. F. *Conduction in Non-Crystalline Materials*. 2nd ed.; Oxford University Press: Oxford, 1993.

(39) Yu, D.; Wang, C.; Wehrenberg, B. L.; Guyot-Sionnest, P. Variable Range Hopping Conduction in Semiconductor Nanocrystal Solids. *Phys. Rev. Lett.* **2004**, *92*, 216802.
(40) Guyot-Sionnest, P. Electrical Transport in Colloidal Quantum Dot Films. *J. Phys. Chem. Lett.* **2012**, *3*, 1169−1175.
(41) Efros, A. L.; Shklovskii, B. I. Coulomb Gap and Low-Temperature Conductivity of Disordered Systems. *J. Phys. C: Solid State Phys.* **1975**, *8*, L49−L51.
(42) Kang, M. S.; Sahu, A.; Norris, D. J.; Frisbie, C. D. Size- and Temperature-Dependent Charge Transport in PbSe Nanocrystal Thin Films. *Nano Lett.* **2011**, *11*, 3887−3892.
(43) Liu, H.; Pourret, A.; Guyot-Sionnest, P. Mott and Efros−Shklovskii Variable Range Hopping in CdSe Quantum Dots Films. *ACS Nano* **2010**, *4*, 5211−5216.
(44) Houtepen, A. J.; Kockmann, D.; Vanmaekelbergh, D. Reappraisal of Variable-Range Hopping in Quantum-Dot Solids. *Nano Lett.* **2008**, *8*, 3516−3520.
(45) Lee, J. S.; Kovalenko, M. V.; Huang, J.; Chung, D. S.; Talapin, D. V. Band-Like Transport, High Electron Mobility, and High Photoconductivity in All-Inorganic Nanocrystal Arrays. *Nat. Nanotechnol.* **2011**, *6*, 348−52.
(46) Choi, J.-H.; Fafarman, A. T.; Oh, S. J.; Ko, D.-K.; Kim, D. K.; Diroll, B. T.; Muramoto, S.; Gillen, J. G.; Murray, C. B.; Kagan, C. R. Bandlike Transport in Strongly Coupled and Doped Quantum Dot Solids: A Route to High-Performance Thin-Film Electronics. *Nano Lett.* **2012**, *12*, 2631−2638.
(47) Oh, S. J.; Berry, N. E.; Choi, J.-H.; Gaulding, E. A.; Lin, H.; Paik, T.; Diroll, B. T.; Muramoto, S.; Murray, C. B.; Kagan, C. R. Designing High-Performance PbS and PbSe Nanocrystal Electronic Devices through Stepwise, Post-Synthesis, Colloidal Atomic Layer Deposition. *Nano Lett.* **2014**, *14*, 1559−1566.
(48) Chung, D. S.; Lee, J.-S.; Huang, J.; Nag, A.; Ithurria, S.; Talapin, D. V. Low Voltage, Hysteresis Free, and High Mobility Transistors from All-Inorganic Colloidal Nanocrystals. *Nano Lett.* **2012**, *12*, 1813−1820.